

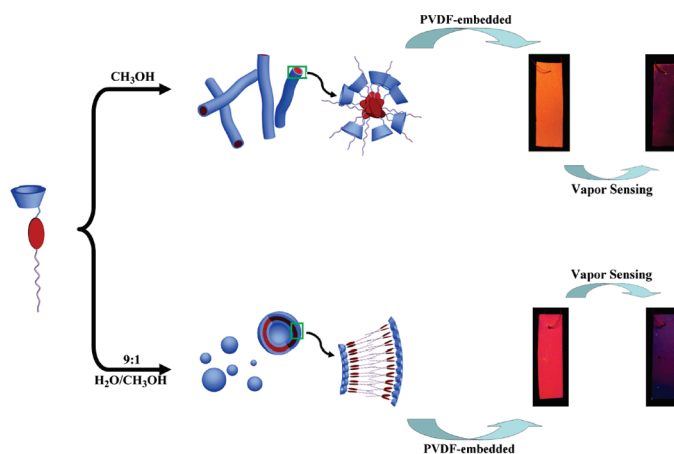
Self-Assembly of Amphiphilic Perylene–Cyclodextrin Conjugate and Vapor Sensing for Organic Amines

Bang-Ping Jiang, Dong-Sheng Guo, and Yu Liu*

Department of Chemistry, State Key Laboratory of Elemento-Organic Chemistry, Nankai University, Tianjin 300071, P. R. China

yuliu@nankai.edu.cn

Received July 26, 2010



An asymmetric, amphiphilic perylene bisimide derivative **1** was synthesized by grafting permethyl- β -cyclodextrin at one side and an octadecyl chain at the other side. Its aggregation capability and morphology, which attract intense interest, were carefully examined by combination of UV–vis, NMR, and fluorescence spectroscopy, DLS, XRD, TEM, and SEM. By adjusting the volume ratio of water and methanol, we are able to control the morphology, benefiting from the amphiphilicity of **1**. Furthermore, the particular resulting aggregates were employed as solid-state fluorescence sensing for organic amines. An improvement of both selectivity and sensitivity is achieved compared to previous publications.

Introduction

Perylene bisimides (PBIs) represent significant photo- and electro-active building blocks in supramolecular dye chemistry.¹ Their assemblies are useful for a wide range of applications,

including liquid crystals,² organogels,³ artificial light harvesting systems,⁴ photoinduced electron transfer systems,⁵ organic electronic devices,⁶ and so on.⁷ Besides the conventional

(1) (a) Würthner, F. *Chem. Commun.* **2004**, 1564–1579. (b) Chen, Z.; Lohr, A.; Saha-Möller, C. R.; Würthner, F. *Chem. Soc. Rev.* **2009**, *38*, 564–584. (c) Zang, L.; Che, Y.; Moore, J. S. *Acc. Chem. Res.* **2008**, *41*, 1596–1608.

(2) Thiebaut, O.; Bock, H.; Grelet, E. *J. Am. Chem. Soc.* **2010**, *132*, 6886–6887.

(3) Würthner, F.; Bauer, C.; Stepanenko, V.; Yagai, S. *Adv. Mater.* **2008**, *20*, 1695–1698.

(4) (a) Tomizaki, K.-Y.; Loewe, R. S.; Kirmaier, C.; Schwartz, J. K.; Retsek, J. L.; Bocian, D. F.; Holten, D.; Lindsey, J. S. *J. Org. Chem.* **2002**, *67*, 6519–6534. (b) De Schryver, F. C.; Vosch, T.; Cotellet, M.; Van der Auweraer, M.; Müllen, K.; Hofkens, J. *Acc. Chem. Res.* **2005**, *38*, 514–522. (c) Baffreau, J.; Ordroneau, L.; Leroy-Lhez, S.; Hudhomme, P. *J. Org. Chem.* **2008**, *73*, 6142–6147.

(5) (a) Prodi, A.; Chiorboli, C.; Scandola, F.; Iengo, E.; Alessio, E.; Dobrawa, R.; Würthner, F. *J. Am. Chem. Soc.* **2005**, *127*, 1454–1462. (b) Céspedes-Guirao, F. J.; Ohkubo, K.; Fukuzumi, S.; Sastre-Santos, A.; Fernández-Lázaro, F. *J. Org. Chem.* **2009**, *74*, 5871–5880.

(6) (a) Kraft, A.; Grimsdale, A. C.; Holmes, A. B. *Angew. Chem., Int. Ed.* **1998**, *37*, 402–428. (b) Weitz, R. T.; Amsharov, K.; Zschieschang, U.; Villas, E. B.; Goswami, D. K.; Burghard, M.; Dosch, H.; Jansen, M.; Kern, K.; Klauk, H. *J. Am. Chem. Soc.* **2008**, *130*, 4637–4645.

(7) (a) Zhan, X.; Tan, Z.; Domercq, B.; An, Z.; Zhang, X.; Barlow, S.; Li, Y.; Zhu, D.; Kippelen, B.; Marder, S. R. *J. Am. Chem. Soc.* **2007**, *129*, 7246–7247. (b) Che, Y.; Yang, X.; Liu, G.; Yu, C.; Ji, H.; Zuo, J.; Zhao, J.; Zang, L. *J. Am. Chem. Soc.* **2010**, *132*, 5743–5750. (c) Wang, W.; Han, J. J.; Wang, L.-Q.; Li, L.-S.; Shaw, W. J.; Li, A. D. Q. *Nano Lett.* **2003**, *3*, 455–458. (d) Wang, W.; Li, L.-S.; Helms, G.; Zhou, H.-H.; Li, A. D. Q. *J. Am. Chem. Soc.* **2003**, *125*, 1120–1121. (e) Spillmann, C. M.; Naciri, J.; Anderson, G. P.; Chen, M.-S.; Ratna, B. R. *ACS Nano* **2009**, *3*, 3214–3220.

intrinsic $\pi \cdots \pi$ stacking interaction between PBI backbones, one area of intense interest in recent years has been the development of several other intermolecular forces that can direct the formation of desirable supramolecular architectures with promising results.^{1a,8} For instance, hydrogen bond is applied to construct J-aggregates that fluoresce with quantum yields of near unity.⁹ A new class of chiral supramolecular liquid-crystalline material has been presented by means of electrostatic self-assembly.¹⁰ Rybtchinski and co-workers designed a comprehensively supramolecular principle that combined amphiphilicity, polymer attachment, $\pi \cdots \pi$ stacking, and coordination interactions to construct optoelectronically active organic materials with different supramolecular morphologies.¹¹ Another specific assembling strategy, grafting macrocyclic compounds onto PBIs, has also been explored by Würthner's group and ours.¹² They reported a series of calixarene–PBI conjugates, where functional dye architectures possessing efficient energy and electron transfer properties were approached, benefiting from well-defined rigid and electron-rich scaffolds of calixarenes.^{12a–f} In our previous works, we prepared two PBI-bridged bis(permethyl- β -cyclodextrins) and found that the assemblies based on PBI–cyclodextrin conjugates can not only present electronic interactions with aromatic guests in aqueous solution but also act as solid-state fluorescence sensor for vapor detection.^{12g,h} It can be therefore inferred that introducing additional anchoring points onto PBIs can not only tailor their aggregation structures but also endow novel probing functions of corresponding assemblies. However, to the best of our knowledge, much less attention has been paid to the latter aspect.¹³

Morphology control of PBI assemblies is also an interesting topic in supramolecular nanomaterials fabrication.¹⁴ Toward this goal, modifying PBIs into amphiphiles by

linking of lipophilic chains at one side and hydrophilic chains at the other side emerges as a smart approach.¹⁵ The nanostructural morphology of asymmetric PBIs can be modulated by solvents, depending on the polarity of the solvents,¹⁶ and also, asymmetric molecules may provide wider options and adaptability for the surface modification to approach optimized sensing sensitivity and selectivity of the nanomaterials thus fabricated.^{15a,17} Zang and co-workers reported a series of ultralong nanobelts and nanofibers fabricated from asymmetric PBI derivatives, exhibiting excellent functions in conductivity and vapor probing.^{7b,13b,13c,15a} An instructive example was presented by Würthner and co-workers that shows hollow vesicles by co-self-assembly of differently shaped PBIs.¹⁸

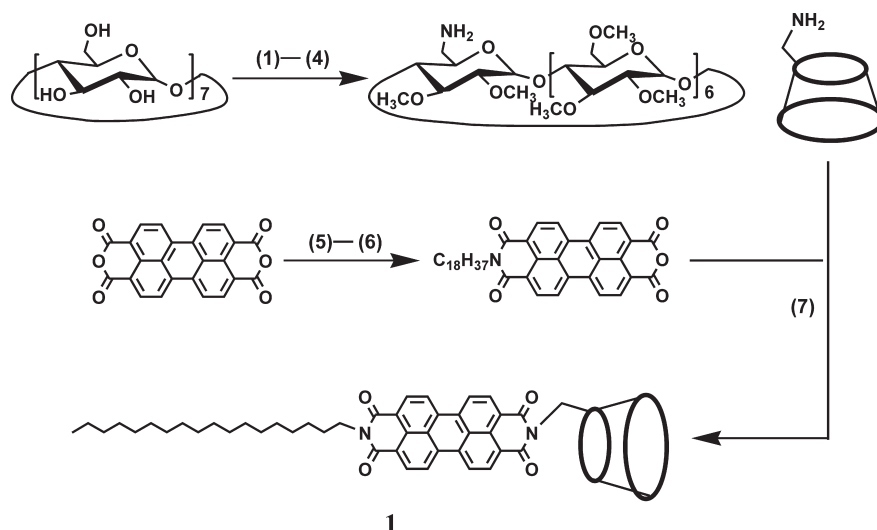
As parts of our ongoing program concerning the supramolecular chemistry of PBI–cyclodextrin conjugates, we developed a brand new asymmetric, amphiphilic PBI derivative **1** by grafting permethyl- β -cyclodextrin at one side and an octadecyl chain at the other side (Scheme 1). The aggregation capability and morphology of **1** is finely modulated by varying solvents, and especially, structural transition from nanorod to sphere is successfully achieved by adjusting the volume ratio of water and methanol. Furthermore, by employing the recognition site of grafted cyclodextrin,¹⁹ the solid-state fluorescence sensing for organic amine vapors was comparatively studied between assemblies derived from solvents of different polarities.

Results and Discussion

Aggregation Capability and Morphology of 1. *N*-Octadecylperylene-3,4:9,10-tetracarboxylic-3,4-permethyl- β -cyclodextrin-9,10-imide (**1**) was synthesized through a total of seven steps as shown in Scheme 1. By grafting a cyclodextrin and an alkyl chain together, **1** exhibits a wide range of solubility in various solvents, including chloroform, toluene, alcohol, and water/methanol (up to 9:1). Differing from PBI-bridged bis(permethyl- β -cyclodextrins),^{12g,h} **1** does not dissolve in pure water, possibly because of two factors: one is the unfavorable effect of long alkyl chain, and the other is the very strong stacking of perylene backbones.¹⁴ The $\pi \cdots \pi$ stacking aggregation behavior of **1** in various solvents was examined by UV–vis spectroscopy as shown in Figure 1. No appreciable stacking of perylenes is observed in toluene, chloroform, acetonitrile, and acetone. UV–vis spectra show three distinguishable absorption bands between 450 and 550 nm with the most absorptivity at the first band. Moderate stacking is observed in methanol, where the absorptivity at 487 and 522 nm decrease obviously with more pronounced variation at 522 nm than at 487 nm, reflecting excitonic coupling between adjacent π -stacking PBIs. When **1** is dissolved in 9:1 water/methanol binary solvent, the spectrum becomes broader, and the maximal absorptivity appears at

- (8) (a) Ehli, C.; Oelsner, C.; Mateo-Alonso, A.; Prato, M.; Schmidt, C.; Backes, C.; Hauke, F.; Hirsch, A.; Guldi, D. M. *Nat. Chem.* **2009**, *1*, 243–249. (b) Hahn, U.; Engmann, S.; Oelsner, C.; Ehli, C.; Guldi, D. M.; Torres, T. *J. Am. Chem. Soc.* **2010**, *132*, 6392–6401. (c) Krieg, E.; Shirman, E.; Weissman, H.; Shimoni, E.; Wolf, S. G.; Pinkas, I.; Rybtchinski, B. *J. Am. Chem. Soc.* **2009**, *131*, 14365–14373. (d) Ryu, J.-H.; Jang, C.-J.; Yoo, Y.-S.; Lim, S.-G.; Lee, M. *J. Org. Chem.* **2005**, *70*, 8956–8962. (9) Kaiser, T. E.; Wang, H.; Stepanenko, V.; Würthner, F. *Angew. Chem., Int. Ed.* **2007**, *46*, 5541–5544. (10) Huang, Y.; Yan, Y.; Smarsly, B. M.; Wei, Z.; Faul, C. F. J. *J. Mater. Chem.* **2009**, *19*, 2356–2362. (11) (a) Baram, J.; Shirman, E.; Ben-Shitrit, N.; Ustinov, A.; Weissman, H.; Pinkas, I.; Wolf, S. G.; Rybtchinski, B. *J. Am. Chem. Soc.* **2008**, *130*, 14966–14967. (b) Golubkov, G.; Weissman, H.; Shirman, E.; Wolf, S. G.; Pinkas, I.; Rybtchinski, B. *Angew. Chem., Int. Ed.* **2009**, *48*, 926–930. (12) (a) Hippus, C.; van Stokkum, I. H. M.; Zangrando, E.; Williams, R. M.; Wykes, M.; Beljonne, D.; Würthner, F. *J. Phys. Chem. C* **2008**, *112*, 14626–14638. (b) Hippus, C.; Schlosser, F.; Vysotsky, M. O.; Böhmer, V.; Würthner, F. *J. Am. Chem. Soc.* **2006**, *128*, 3870–3871. (c) Siekierzycka, J. R.; Hippus, C.; Würthner, F.; Williams, R. M.; Brouwer, A. M. *J. Am. Chem. Soc.* **2010**, *132*, 1240–1242. (d) Anh, N. V.; Schlosser, F.; Groeneveld, M. M.; van Stokkum, I. H. M.; Würthner, F.; Williams, R. M. *J. Phys. Chem. C* **2009**, *113*, 18358–18368. (e) Hippus, C.; van Stokkum, I. H. M.; Gsänger, M.; Groeneveld, M. M.; Williams, R. M.; Würthner, F. *J. Phys. Chem. C* **2008**, *112*, 2476–2486. (f) Vysotsky, M. O.; Böhmer, V.; Würthner, F.; You, C.-C.; Rissanen, K. *Org. Lett.* **2002**, *4*, 2901–2904. (g) Wang, K.-R.; Guo, D.-S.; Jiang, B.-P.; Sun, Z.-H.; Liu, Y. *J. Phys. Chem. B* **2010**, *114*, 101–106. (h) Liu, Y.; Wang, K.-R.; Guo, D.-S.; Jiang, B.-P. *Adv. Funct. Mater.* **2009**, *19*, 2230–2235. (13) (a) Wang, B.; Yu, C. *Angew. Chem., Int. Ed.* **2010**, *49*, 1485–1488. (b) Che, Y.; Yang, X.; Loser, S.; Zang, L. *Nano Lett.* **2008**, *8*, 2219–2223. (c) Che, Y.; Zang, L. *Chem. Commun.* **2009**, 5106–5108. (14) Balakrishnan, K.; Datar, A.; Naddo, T.; Huang, J.; Oitker, R.; Yen, M.; Zhao, J.; Zang, L. *J. Am. Chem. Soc.* **2006**, *128*, 7390–7398. (15) (a) Che, Y.; Datar, A.; Balakrishnan, K.; Zang, L. *J. Am. Chem. Soc.* **2007**, *129*, 7234–7235. (b) Gebers, J.; Rolland, D.; Frauenrath, H. *Angew. Chem., Int. Ed.* **2009**, *48*, 4480–4483.

- (16) Yang, X.; Xu, X.; Ji, H.-F. *J. Phys. Chem. B* **2008**, *112*, 7196–7202. (17) Hill, J. P.; Jin, W.; Kosaka, A.; Fukushima, T.; Ichihara, H.; Shimomura, T.; Ito, K.; Hashizume, T.; Ishii, N.; Aida, T. *Science* **2004**, *304*, 1481–1483. (18) (a) Zhang, X.; Chen, Z.; Würthner, F. *J. Am. Chem. Soc.* **2007**, *129*, 4886–4887. (b) Zhang, X.; Rehm, S.; Safont-Sempere, M. M.; Würthner, F. *Nat. Chem.* **2009**, *1*, 623–629. (19) (a) Szejtli, J. *Chem. Rev.* **1998**, *98*, 1743–1753. (b) Rekharsky, M. V.; Inoue, Y. *Chem. Rev.* **1998**, *98*, 1875–1918. (c) Liu, Y.; Chen, Y. *Acc. Chem. Res.* **2006**, *39*, 681–691. (d) Connors, K. A. *Chem. Rev.* **1997**, *97*, 1325–1357.

SCHEME 1. Synthetic Route of **1**^a

^a(1) NaOH, tosyl chloride; (2) NaN₃/70 °C; (3) NaH, CH₃I; (4) LiAlH₄; (5) KOH, CH₃COOH/90 °C; (6) 1-octadecanamine/90 °C; (7) Zn(CH₃COO)₂/100 °C.

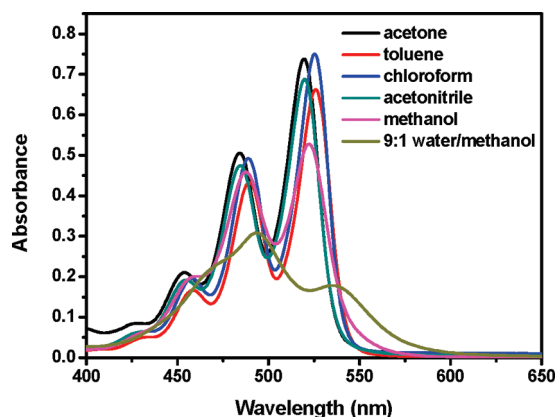


FIGURE 1. UV-vis spectra of **1** (1.0×10^{-5} M) in different solvents at 25 °C.

the second band, which indicates more pronounced $\pi \cdots \pi$ stacking aggregation of **1**.

The solvent-dependent stacking behavior of **1** was also validated by NMR method. Owing to poor solubility in water/methanol binary solvents, ¹H NMR spectra of **1** were comparatively studied in CDCl₃ and CD₃OD (Figure S5 in Supporting Information). In CDCl₃, a simple pattern of sharp signals for the perylene protons is observed, indicating that **1** exists in the monomeric form (or at most a very low aggregated form) at such a high concentration of 3 mM, whereas in CD₃OD, the signals are drastically broadened and suffer pronounced upfield shifts as a result of the π -stacking ring current.^{7c,d,20}

To gain more insight into the thermodynamics of the aggregation process of **1** in pure methanol, both concentration- and temperature-dependent UV-vis spectra were performed (Figure 2). At low concentration of 2.0×10^{-6} M, **1** is judged as a nonaggregated or low aggregated state according to the

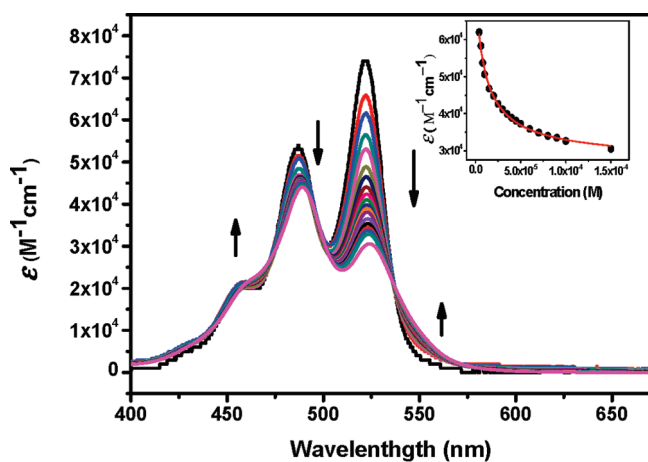
well-resolved vibronic structure observed in the absorption spectrum, and the maximal absorptivity appears at 522 nm.²¹ Both of the apparent absorption coefficients of 522 and 487 nm decrease upon increasing concentrations, but with more pronounced variation at 522 nm than at 487 nm, therefore leading to the maximal absorptivity migrating from 522 to 487 nm. In addition, a new shoulder appears at about 550 nm with increasing concentrations. These phenomena reflect the stronger and stronger electronic coupling between the PBI backbones with the enhancement of concentrations. It can be seen from the temperature-dependent UV-vis spectra that the aggregate of **1** melts gradually when the temperature rises from 5 to 60 °C, indicating the enthalpy-driven process of π -stacking aggregation of PBIs.^{21b}

Taking the amphiphilic structure of **1** into account, the aggregation of **1** was carefully examined in water/methanol binary solvents with different volume ratios, although unfortunately **1** does not dissolve in pure water. As shown in Figure 3a, the absorption band at 522 nm decreases remarkably upon tuning water components (0:10–3:7), whereas the absorption band at 488 nm changes little. A special case appears in 4:6 water/methanol where **1** was precipitated from mother liquor, that is, **1** forms an insoluble aggregate in this environment.²² Further increasing water components (5:5–9:1) recovers the solubility of **1** and leads to stronger aggregation with broader absorption bands. Comparing the UV-vis spectra in pure methanol and 9:1 water/methanol, both absorption bands shift from 488 and 522 nm to 494 and 535 nm. A similar result was also detected in the fluorescence spectra (Figure 3b). The monomer emission decreases, while the excimer emission (600–850 nm), implying formation of oligomer aggregate, increases gradually along with enriching

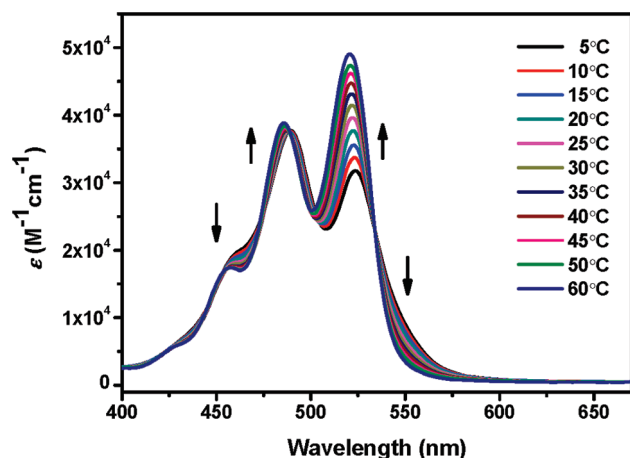
(20) (a) Shaller, A. D.; Wang, W.; Gan, H.; Li, A. D. Q. *Angew. Chem., Int. Ed.* **2008**, *47*, 7705–7709. (b) Li, A. D. Q.; Wang, W.; Wang, L.-Q. *Chem.—Eur. J.* **2003**, *9*, 4594–4601.

(21) (a) Sadrai, M.; Hadel, L.; Sauers, R. R.; Husain, S.; Krogh-Jespersen, K.; Westbrook, J. D.; Bird, G. R. *J. Phys. Chem.* **1992**, *96*, 7988–7996. (b) Chen, Z.; Stepanenko, V.; Dehm, V.; Prins, P.; Siebels, L. D. A.; Seibt, J.; Marquetand, P.; Engel, V.; Würthner, F. *Chem.—Eur. J.* **2007**, *13*, 436–449.

(22) For the poor solubility, it may be interpreted in terms of the after-mentioned aggregation size that large aggregates are prone to fall out of solution.



(a)

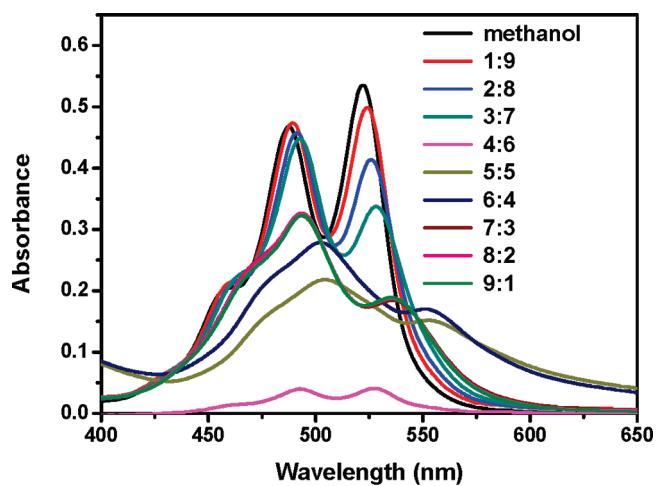


(b)

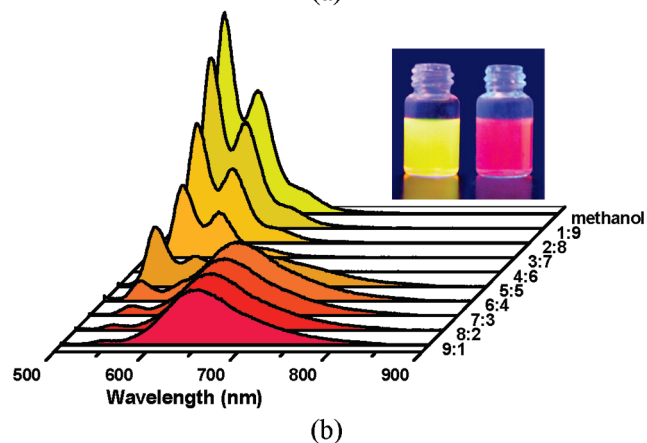
FIGURE 2. (a) Concentration-dependent UV-vis spectra of **1** (2.0×10^{-6} to 1.5×10^{-4} M) in pure methanol at 25 °C. Arrows indicate the changes upon increasing the concentration. Inset: the variation of the apparent absorption coefficients at 522 nm. (b) Temperature-dependent UV-vis spectra of **1** from 5 to 60 °C (2.0×10^{-5} M) in pure methanol. Arrows indicate the spectra changes upon increasing the temperature.

water components. A significant color change of fluorescence takes place, with yellow emission in pure methanol and red emission in 9:1 water/methanol. It can be therefore deduced from the present results that **1** exhibits much stronger aggregation capability in 9:1 water/methanol than in pure methanol. In addition, the distinguishable aggregation capabilities were further validated by XRD experiments, showing $\pi \cdot \cdot \cdot \pi$ stacking distance of 4.0 Å in pure methanol, and 3.4 Å in 9:1 water/methanol (Figure S10 in Supporting Information).

The concentration-dependent UV-vis spectra of **1** were also performed in 9:1 water/methanol (Figure S7 in Supporting Information). However, the apparent absorption coefficients experience no appreciable change in the concentration region from 4.0×10^{-6} to 1.0×10^{-4} M, indicating extremely strong aggregation capability. Comparing with previous PBI-bridged bis(permethyl- β -cyclodextrins),^{12g,h} **1** possesses much stronger aggregation ability in aqueous solution. This may reasonably originate from two factors: one is that grafting only one cyclodextrin unit brings about smaller steric hindrance,



(a)



(b)

FIGURE 3. Solvent-dependent UV-vis (a) and fluorescence (b) spectra of **1** (1.0×10^{-5} M) in the water/methanol binary solvents at 25 °C, $\lambda_{\text{ex}} = 490$ nm. Inset shows the fluorescence photographs of **1** (1.0×10^{-4} M) in pure methanol (left) and 9:1 water/methanol (right) upon irradiation at 365 nm.

and the other is that the amphiphilic structure prompts stronger stacking, as hydrophobic interaction between the linear side chains is highly cooperative with the $\pi \cdot \cdot \cdot \pi$ interaction between perylene planes.^{14,16}

To give further insight into the shape, size, and size distribution of the aggregates, TEM and SEM images of **1** were recorded in methanol and 4:6 and 9:1 water/methanol, respectively (Figure 4). It is found that the aggregation morphology of **1** is dominantly solvent-dependent; **1** shows nanorod aggregation (averaged length of 70 nm) in pure methanol, chunky nanostructure (averaged length of 500 nm and width of 90 nm) in 4:6 water/methanol, and spherical morphology (averaged diameter of 60 nm) in 9:1 water/methanol. Combining the microscopy images and aforementioned spectral results and also taking the intrinsic amphiphilic characteristics of **1** into account, we propose the possible aggregation models in different solvents as shown in Scheme 2. In pure methanol, the PBI backbones of **1** π -stack in a rotational manner (the adjacent planes are parallel to each other), forming the core of a nanorod, where the cyclodextrin grafts and alkyl chains point outside randomly. In 4:6 water/methanol, amphiphilic aggregation takes place, where the hydrophilic cyclodextrins point to one side and the hydrophobic alkyls point to the other side, forming

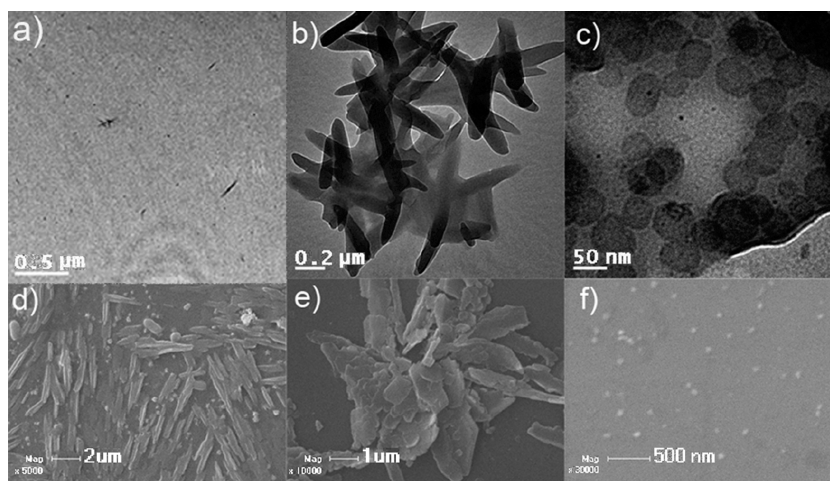
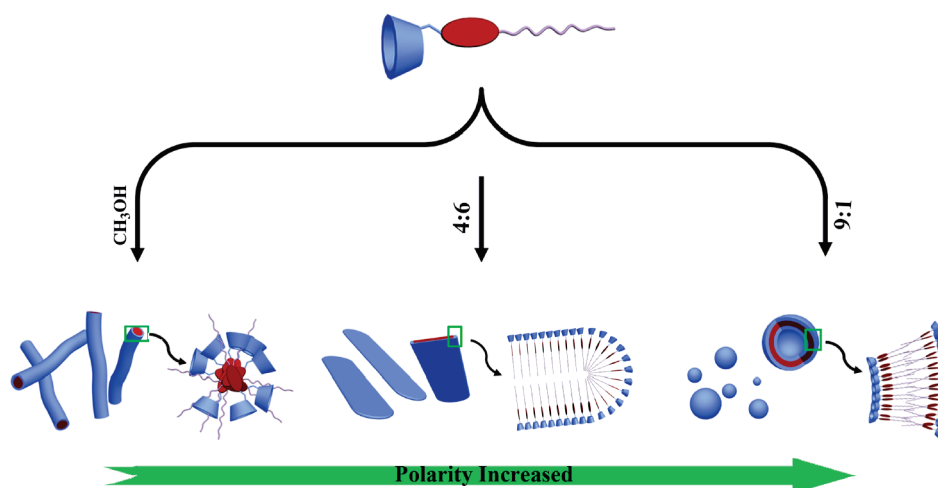


FIGURE 4. Solvent-dependent TEM (a–c) and SEM (d–f) images, from left to right: methanol, 4:6 water/methanol, 9:1 water/methanol.

SCHEME 2. Assembly Models of 1 in Water/Methanol Mixed Solvents with Various Compositions^a



^a1D nanorod (pure methanol, left), chunky nanostructure like floppy micelle (4:6 water/methanol, middle), and spherical micelle (9:1 water/methanol, right).

large chunky aggregates like floppy micelles. It should be mentioned that the aggregation at 4:6 ratio is a static (non-equilibrium) structure owing to its poor solubility. This is in accordance with a previous result by Zang and co-workers that fast aggregation is disadvantageous for a molecular assembly to grow along one direction and advantageous to form chunky assemblies.¹⁴ In 9:1 water/methanol, the PBI backbones π -stack with a certain angle formed between adjacent planes, the hydrophilic cyclodextrins point to one side, and the hydrophobic alkyls point to the other side, and therefore the hydrophilic/hydrophobic interface becomes curved, resulting in the spherical aggregation. The measured diameters of the aggregates exceeded the corresponding extended molecular length (approximately 5 nm), suggesting that these aggregates are vesicular entities rather than simple micelles.²³ It should be stated that the interpretation of the solution-phase assembly only using dry TEM and SEM can be problematic, because drying can have significant influence on the aggregation morphology of **1**. The size of vesicles was

further identified by DLS analysis, giving an average hydrodynamic diameter of 75 nm (Figure S9 in Supporting Information).²⁴ A sharp size distribution indicates that the uniform vesicles are ubiquitous in aqueous solution. The amphiphilic aggregation of **1** in 9:1 water/methanol can also be reflected from the curved surface of the solution, as a result of the decrease of surface tension (inset photograph in Figure 3). Such transition of aggregation morphology from nonamphiphilic nanorod, to floppy micelle, to vesicle, accompanied by the decrease of curvature, is acceptable as **1** exhibits more and more pronounced amphiphilicity with the increase of solvent polarity.

Solid-State Fluorescence Sensing for Vapor Detection. The aggregates of **1** were embedded in the poly(vinylidene fluoride) (PVDF) membrane from pure methanol and 9:1 water/methanol, respectively, resembling the previous PBI-bridged bis(permethyl- β -cyclodextrins).^{12h} The UV-vis and fluorescence spectra of the PVDF membrane-embedded **1** were prerequisitely recorded, referring to the spectra in chloroform (Figure 5). The broadened

(23) Lee, M.; Lee, S.-J.; Jiang, L.-H. *J. Am. Chem. Soc.* **2004**, *126*, 12724–12725.

(24) It is reasonable that the diameter measured by TEM is smaller than that of DLS. The spherical micelle in the process of TEM sample preparation loses solvent, which leads to its shrinkage.

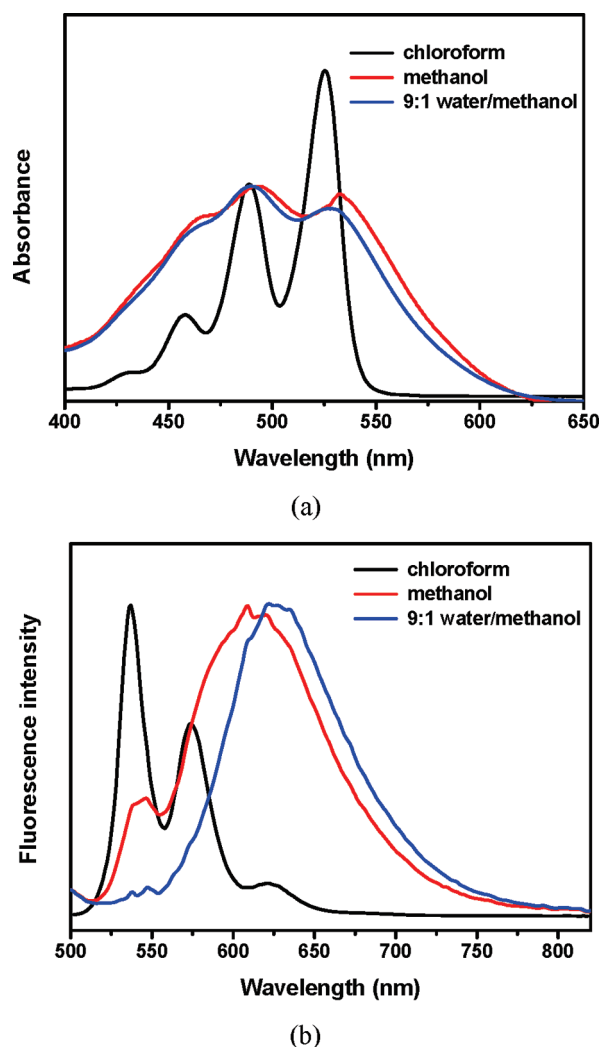


FIGURE 5. UV-vis (a) and fluorescence (b) spectra of **1** in chloroform (1.0×10^{-5} M) and the PVDF membrane-embedded **1** from methanol and 9:1 water/methanol, respectively, $\lambda_{\text{exc}} = 490$ nm.

absorption bands and the decreased absorptivities clearly are responses to the aggregation state of **1** from both pure methanol and 9:1 water/methanol. Appreciable difference of solid-state fluorescence is observed for **1** from pure methanol and 9:1 water/methanol. The PVDF-embedded **1** from pure methanol shows a major excimer emission at 609 nm, together with a minor monomer emission at 545 nm, whereas **1** from 9:1 water/methanol shows only excimer emission at 625 nm. The excimer emission of **1** from 9:1 water/methanol is relatively bathochromic in comparison to that from pure methanol, concurrently with a narrower band, which indicates better exciton migration originating from stronger $\pi \cdots \pi$ interaction and more well-organized molecular aggregation.^{13b} As a result of the distinguishable aggregation states, the vapor sensing behaviors for various volatile organic compounds are different for **1** from methanol and 9:1 water/methanol (Figure 6). For most substrates, the fluorescence quenching of **1** from 9:1 water/methanol is more pronounced than that of **1** from methanol, exhibiting better sensitivity. It is reasonably acceptable that stronger $\pi \cdots \pi$ interaction promotes the longer-range molecular arrangement leading to enhanced exciton migration (via intermolecular π -electronic coupling) along the long axis of aggregation, which

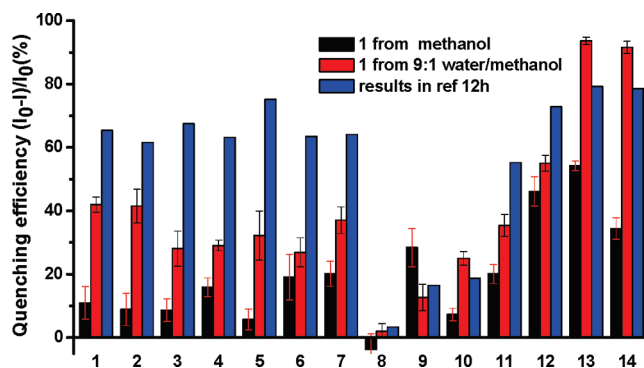


FIGURE 6. Fluorescence response of **1** and PBI-bridged bis(permethyl- β -cyclodextrins)^{12h} to the saturated vapors of various amines, nitro-based compounds and general organic solvents with a response time of 10 s: 1, toluene; 2, chlorobenzene; 3, nitroethane; 4, nitromethane; 5, acetonitrile; 6, methanol; 7, chloroform; 8, nitrobenzene; 9, hydrazine hydrate; 10, benzylamine; 11, triethylamine; 12, butylamine; 13, aniline; 14, *o*-methyl-aniline. Error bar: standard deviation.

can be disturbed by fewer analyte molecules, enabling amplification in fluorescence quenching.^{14,25}

Comparing the sensing results of the PVDF-embedded **1** from 9:1 water/methanol with those of previous PBI-bridged bis(permethyl- β -cyclodextrins),^{12h} it is found that the probing selectivity for organic amines (especially for butylamine, aniline, and *o*-methyl-aniline) relative to other common organic reagents was improved to some extent. Taking aniline/toluene pairs as example, the solid-state fluorescence of PBI-bridged bis(permethyl- β -cyclodextrins) is quenched 79% by aniline and 65% by toluene, giving a selectivity of 1.2; the solid-state fluorescence of **1** is quenched $94 \pm 1\%$ by aniline and $42 \pm 2\%$ by toluene, giving a selectivity of 2.2. In fact, the real selectivity should be much higher than the observed one when taking into account the saturated vapor pressures (880 ppm for aniline and 38000 ppm for toluene; see Table S1 in Supporting Information for saturated vapor pressures of the other analytes). The sensitivity can be reflected from the concentration-dependent fluorescence response of **1** for aniline, quenched 20% with a vapor pressure of 44 ppm (Figure S11 in Supporting Information). Two factors lead to the fluorescence quenching upon binding analytes: one is the photoinduced electron transfer from analytes to PBI probe, and the other is that inclusion of analytes into the cyclodextrin cavity disturbs the well-ordered $\pi \cdots \pi$ aggregation of PBI backbones. For analytes of general organic solvents and nitro-based compounds, the fluorescence quenching of PBI aggregates should mainly be ascribed to the latter reason. The aggregation capability of **1** is much stronger than that of PBI-bridged bis(permethyl- β -cyclodextrins) as proved above, and it is much more difficult for inclusion of analytes into the cyclodextrin cavity to alter the π -stacking of **1** than PBI-bridged bis(permethyl- β -cyclodextrins). As a result, the fluorescence quenching efficiencies by these common organic reagents decrease remarkably from PBI-bridged bis(permethyl- β -cyclodextrins) to **1**. In other words, enhancing the π -stacking strength of PBI back-

(25) (a) Swager, T. M. *Acc. Chem. Res.* **2008**, *41*, 1181–1189. (b) Thomas, S. W., III; Joly, G. D.; Swager, T. M. *Chem. Rev.* **2007**, *107*, 1339–1386. (c) McQuade, D. T.; Pullen, A. E.; Swager, T. M. *Chem. Rev.* **2000**, *100*, 2537–2574.

bones can effectively inhibit the background interference of common organic reagents. The work is ongoing to avoid the steric hindrance of cyclodextrin as much as possible by elongating the spacer between cyclodextrin and PBI.

Among these organic amines detected by the PVDF-embedded **1** from 9:1 water/methanol, aniline and *o*-methyl-aniline show better quenching efficiencies, $94 \pm 1\%$ and $92 \pm 2\%$, respectively. This is reasonably ascribed to higher binding affinity of cyclodextrins for aromatic guests than for aliphatic ones. The fluorescence intensity is quenched only $25 \pm 2\%$ by benzylamine, although it is also aromatic owing to its weak electron-donor capability. Hydrazine hydrate and triethylamine are typically robust electron donors; however, they quench fluorescence of **1** merely $13 \pm 4\%$ and $35 \pm 4\%$, which also reflects the binding selectivity of cyclodextrins in the present sensing system. It is indeed a challenge that distinguishing aromatic and aliphatic amines by the solid-state fluorescence sensing species based on PBIs up to now.^{12h,13b}

Conclusions

In summary, we have successfully synthesized an asymmetrical, amphiphilic PBI–cyclodextrin conjugate **1** by grafting permethyl- β -cyclodextrin at one side and an octadecyl chain at the other side. Its aggregation capability is controlled by the polarization of solvents, while the aggregation morphology is modulated by the polarity of solvents, ranging from nanorod to vesicle. Aggregates of **1** exhibit benign solid-state emission, which can act as fluorescence sensory material for vapor detection, together with the specific binding sites offered by grafted cyclodextrins. Compared with previous results by PBI-bridged bis(permethyl- β -cyclodextrins),^{12h} **1** presents not only better sensitivity but also higher selectivity for organic amines, which inspires us that strengthening π -stacking of PBI backbones can effectively improve the probing property of PBI–cyclodextrin conjugates. Endeavors to further construct aggregates based on PBI–cyclodextrin conjugates are in progress, in which of particular interest is exploring fascinating species with high sensitivity and selectivity for detecting specialized analytes.

Experimental Section

Materials. All chemicals used are reagent grade unless noted otherwise. Perylene-3,4,9,10-tetracarboxylic acid dianhydride and octadecylamine were purchased from commercial resources and used without further purification. 6-Deoxy-6-amino-permethyl- β -cyclodextrin (PMCD-NH₂) was synthesized according to the procedure in the literature from natural β -cyclodextrin.²⁶ *N*-Octadecylperylene-3,4:9,10-tetracarboxylic-3,4-anhydride-9,10-imide (OC-PBI) was synthesized and purified according to the reported procedures.²⁷ Pyridine was dried over CaH₂ for 2–3 days and then distilled prior to use. The poly(vinylidene fluoride) (PVDF) membrane was purchased from commercial resources.

Synthesis of *N*-Octadecylperylene-3,4:9,10-tetracarboxylic-3,4-permethyl- β -cyclodextrin-9,10-imide (1**).** PMCD-NH₂ (500 mg, 0.35 mmol), OC-PBI (227 mg, 0.35 mmol), and zinc acetate (77 mg,

0.35 mmol) were mixed in pyridine (150 mL). The reaction mixture was heated at 100 °C under N₂ for 48 h. After cooling to room temperature, the solvent was removed at reduced pressure, and the residue was dissolved in chloroform, washed with water, dried over Na₂SO₄, and evaporated to dryness under vacuum. The residue was purified by silica gel column chromatography using ethyl acetate as the eluent to give the product as a red powder (310 mg) at a yield of 43%. ¹H NMR (400 MHz, CDCl₃, δ , ppm) 8.69 (m, 8H), 5.26–4.96 (m, 7H), 4.73 (d, 2H), 4.32 (m, 1H), 4.21 (t, 2H), 4.01–2.67 (m, 99H), 1.76 (m, 2H), 1.34 (m, 30H), 0.88 (t, 3H); ¹³C NMR (100 MHz, CDCl₃, δ , ppm) 163.4, 163.3, 134.8, 134.3, 131.5, 129.4, 126.5, 123.6, 123.3, 123.2, 123.0, 99.7, 99.1, 98.7, 98.6, 98.5, 85.1, 82.0, 79.3, 71.6, 71.1, 71.0, 70.8, 70.5, 61.5, 61.4, 59.1, 58.7, 58.6, 58.5, 41.9, 40.8, 32.0, 29.7, 28.1, 22.8, 22.5, 14.1. MALDI-MS: calcd for C₁₀₄H₁₅₄N₂O₃₈Na⁺, 2062.0072; found 2061.969. Anal. Calcd for C₁₀₄H₁₅₄N₂O₃₈: C 61.22, H 7.61, N 1.37. Found: C 61.19, H 7.65, N 1.34.

The sample for TEM measurements was prepared by dropping the solution onto a copper grid. The concentrations of **1** in methanol, 4:6 water/methanol, and 9:1 water/methanol are 5.0×10^{-5} , 1.0×10^{-5} , and 1.0×10^{-5} M, respectively. Scanning electron microscopic (SEM) images are recorded. The concentrations of **1** in methanol, 4:6 water/methanol, and 9:1 water/methanol are all 1.0×10^{-4} M.

The dynamic light scattering (DLS) was performed at 636 nm. The sample solution of **1** (1.0×10^{-5} M) in 9:1 water/methanol for DLS measurements was prepared by filtering the solution through a 450 nm filter into a clean scintillation vial.

PVDF Membrane-Embedded **1 and Solid-State Fluorescence Sensing Experiments.** The solid-state fluorescence sensing experiments were performed as follows: (i) the PVDF membrane was immersed in 9:1 water/methanol with **1** at 1.0×10^{-4} M and in methanol with **1** at 1.0×10^{-3} M for 2 h, and then the PVDF membrane was air-dried and tailored to the proper size based on the front surface accessory on a fluorescence spectrometer; (ii) to prevent direct contact of the film with the analytes, cotton thread was used to hang the membrane in the jar when detecting; (iii) the solid-state fluorescence spectra were measured immediately after immersing inside a sealed jar (100 mL) containing small amounts of the amines and nitro-based compounds. Before use the jar was sealed overnight to achieve vapor saturation inside. The exposure time was determined by stopwatch. The sensing sensitivities were performed: injection of 5 mL of saturated aniline vapor (880 ppm) into the 100 mL sealed-jar will produce a vapor pressure of 44 ppm.

Standard Deviation. To calculate the standard deviations of the solid-state fluorescence sensing experiments using eq 1, we performed four individual tests for each gas.

$$S = \sqrt{\frac{\sum (X_i - \bar{X})^2}{(n-1)}} \quad (1)$$

where S = standard deviation in gas sensing tests, Σ = summation, n = number of tests, X_i = each individual quenching efficiency in gas sensing tests, and \bar{X} = mean average of quenching efficiency in gas sensing tests.

Acknowledgment. This work was supported by the 973 Program (2006CB932900), NNSFC (Nos. 20703025, 20721062 and 20932004) and 111 Project (B06005), which are gratefully acknowledged.

Supporting Information Available: NMR, MALDI-MS spectra of **1**, and other data as described in the text. This material is available free of charge via the Internet at <http://pubs.acs.org>.

(26) (a) Hocquelet, C.; Blu, J.; Jankowski, C. K.; Arseneau, S.; Buisson, D.; Mauclaire, L. *Tetrahedron* **2006**, *62*, 11963–11971. (b) Reetz, M. T.; Waldvogel, S. R. *Angew. Chem., Int. Ed.* **1997**, *36*, 865–867.

(27) (a) DeSaja-Gonzalez, J.; Aroca, R.; Nagao, Y.; A DeSaja, J. *Spectrochim. Acta, Part A* **1997**, *53*, 173–181. (b) Wescott, L. D.; Mattern, D. L. *J. Org. Chem.* **2003**, *68*, 10058–10066.